Journal of Nuclear Materials 402 (2010) 179–185

Contents lists available at ScienceDirect

Journal of Nuclear Materials

journal homepage: www.elsevier.com/locate/jnucmat

An analytical study of gas-bubble nucleation mechanisms in uranium-alloy nuclear fuel at high temperature ☆

J. Rest *

Argonne National Laboratory, 9700 S. Cass Ave., Argonne, IL 60439, USA

ARTICLE INFO

Article history:
Received 19 October 2009
Accepted 24 May 2010

ABSTRACT

A multi-atom gas-bubble nucleation mechanism in uranium-alloy nuclear fuel operating in the high-temperature equilibrium gamma phase is proposed based on interpretation of measured intragranular bubble-size distribution data. This model is contrasted with the conventional two-atom nucleation mechanism within the context of a mechanistic calculation of the fission-gas bubble-size distribution. The results of the analysis enable the calculation of safety margins for unrestrained fuel swelling. These safety margins contain an uncertainty primarily tied to uncertainties in the values of the volume and Xe diffusion coefficients.

1. Introduction

Fig. 1 shows an SEM micrograph of U–Zr–Pu uranium alloy fuel [1] irradiated at temperatures above that at which the equilibrium gamma phase forms (>660 °C). Swelling of this material is predominantly due to the growth of fission-gas bubbles. Its fission gas behavior is characterized by high mobility, and is typical of most uranium metal alloys irradiated at the relatively high temperatures where it exists in the equilibrium γ-U–Zr–Pu phase. As seen in Fig. 1, the bubbles in this material comprise a relatively broad size range. Some of the larger bubbles have a sinuous plastic-like appearance, indicative of high mobility. A number of coalescence events are apparent, and some of the larger bubbles appear to be growing into the smaller neighboring bubbles.

Most attempts at describing intragranular gas-bubble nucleation in nuclear fuels at higher temperatures have relied on a homogeneous [2], or heterogeneous [3] two-atom mechanism. In general, it is assumed that two-atoms that come together in the presence of vacancies or vacancy clusters becomes a stable nucleus. At lower temperature, due to the relatively strong effect of irradiation-induced re-solution, the number of nucleated bubbles increases due to the increase in the effective gas generation rate [4]. In theory (i.e., as a postulate), the number of nuclei will increase until newly created gas atoms are more likely to be captured by an existing nucleus than to meet other gas atoms and form new nuclei [2,5]. In practice (i.e., as an implemented calculation), due to the coarsening of the bubble-size distribution the two-atom nucleation process continues throughout the irradiation.

If both bubble motion and coalescence are neglected, the rate equation describing the time evolution of the density of gas in intragranular bubbles is given by

$$\frac{d[m_b(t)c_b(t)]}{dt} = 16\pi f_n D_g r_g c_g(t)c_g(t) + 4\pi r_b(t) D_g c_g(t) c_b(t) - b m_b(t) c_b, \quad (1)$$

where c_g, c_b are the density of gas atoms and bubbles, respectively, r_g is the radius of a gas atom, m_b is the average number of gas atoms per bubble, D_g is the gas-atom diffusion coefficient, b is the gas-atom re-solution rate from bubbles, and f_n, the so-called nucleation factor, is the probability that two gas atoms that come together stick long enough to form a stable bubble nucleus. Often, f_n is interpreted as the probability that there are sufficient vacancies or vacancy clusters in the vicinity of the two-atom to form a stable nucleus. For example, for heterogeneous bubble nucleation along fission tracks in UO_2 f_n is approximately the average volume fraction of fission tracks $\approx 10^{-4}$. The three terms on the right hand side of Eq. (1) represent, respectively, the change in the density of gas in intragranular bubbles due to bubble nucleation, gas-atom diffusion to bubbles of radius, r_b, and the loss of gas atoms from bubbles due to irradiation-induced re-solution.

An implicit assumption in Eq. (1) is that once a two-atom nucleus forms it grows instantaneously to an m-atom bubble. Values of f_n ranging from 10^{-7} to 10^{-2} have been proposed which makes the nucleation factor little more than an adjustable parameter [6]. A substantial contribution to the spread of reported values for f_n is that most models describe the time evolution of mean values of c_b and r_b which are compared to the respective mean values

☆ Work supported by US Department of Energy, Office of Global Threat Reduction, National Nuclear Security Administration (NNSA), under Contract DE-AC-02-06CH11357.

* Tel.: +1 630 252 5026; fax: +1 630 252 5161.
E-mail address: jrest@anl.gov

0022-3115/$ - see front matter © 2010 Elsevier B.V. All rights reserved.
doi:10.1016/j.jnucmat.2010.05.022

of the measured quantities (comparing model predictions with average quantities is by far the dominant validation technique reported in the literature). It has recently been shown that a substantial increase in validation leverage is secured with the use of bubble-size distributions compared with the use of mean values [7]. The results of a series of calculations made with paired values of critical parameters, chosen such that the calculation of average quantities remains unchanged, demonstrated that the calculated distribution undergoes significant changes in shape as well as position and height of the peak. As such, a capacity to calculate bubble-size distributions along with the availability of measured distributions goes a long way in validating not only values of key materials properties and model parameters, but also proposed fuel behavioral mechanisms.

More recently, application of a general form of the kinetic coefficients of the Fokker–Planck equation describing gas-bubble nucleation in supersaturated solution of vacancies, interstitials, and gas atoms has shown that high densities of gas atoms collected in the nucleated bubbles considerably decrease the critical bubble size and its nucleation barrier [8]. The two-atom nucleation model, described above, is not consistent with this finding. As an approach to circumventing this discrepancy, in what follows a multi-atom bubble nucleation mechanism is proposed and implemented into a mechanistic calculation of the intragranular fission-gas bubble-size distribution. This approach is analogous to the intergranular multi-atom bubble nucleation mechanism utilized for the U–Mo alloy in the low-temperature irradiation-stabilized gamma phase [7]. The results of the calculations are compared to a measured bubble-size distribution in U–10Mo irradiated at relatively high temperature to 4% U atom burnup. The multi-atom nucleation model is compared to the two-atom model within the context of the data and implications of each mechanism for the observable quantities are discussed.

In the next section, a multi-atom nucleation mechanism is formulated. Section 3 presents an outline for a calculation of the time evolution of the bubble-size distribution. In Section 4, a discussion is presented of processes that lead to coarsening of the as-nucleated bubble distribution. In Section 5, model calculations are used to interpret a measured distribution in U–8Mo uranium alloy fuel irradiated to 4%U burnup at 850 K. In addition, in this section a comparison between the multi-atom and two-atom nucleation mechanism is attempted. An application of this formulation to the calculation of gas-driven fuel swelling safety margins is described in Section 6. Finally, conclusions are presented in Section 7.

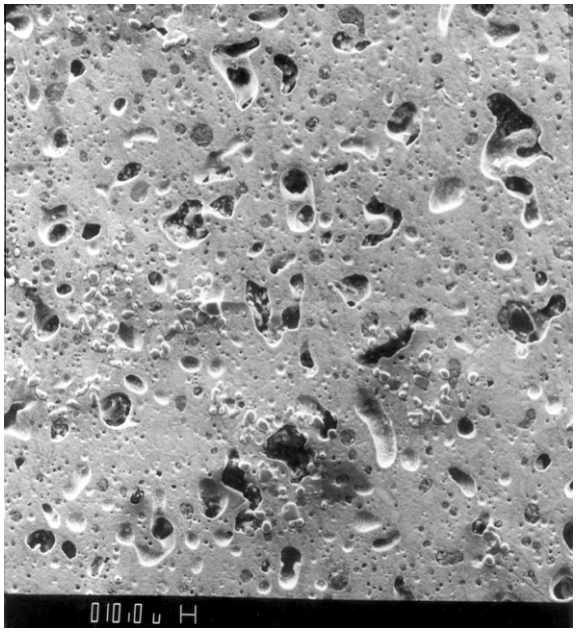

Fig. 1. SEM micrograph of γ-U–Zr–Pu uranium alloy fuel [1].

2. A multi-atom nucleation mechanism

Fission gas Xe and Kr are generated in a nuclear fuel at the rate of about 0.25–0.30 atoms per fission as a result of decay of the primary fission products. About 7 times more Xe is produced than Kr. These gas atoms are very insoluble in the fuel in that they do not react chemically with any other species. Thus, left as an interstitial, due to their relatively large size, they produce a strain in the material. In order to lower the energy of the system and to minimize the strain, the gas atoms tend to relocate in areas of decreased density, such as in vacancies and/or vacancy clusters. For example, in UO_2 gas atoms have been calculated to sit in neutral tri-vacancy sites consisting of two oxygen and one uranium ions [9]. Given enough energy via thermal fluctuations, and/or via irradiation, the gas atoms can hop randomly from one site to another and thus diffuse through the material. The gas atom/vacancy complexes can combine forming clusters of gas atoms and vacancies. If enough gas atoms come together the object is transformed into a gas bubble which, under equilibrium conditions, sits in a strain free environment. This process of forming gas bubbles is termed gas-bubble nucleation.

According to phase transition theory, at relatively large supersaturations a system transforms not by atom-to-atom growth, but simultaneously as a whole. In other words, the system is unstable against transformations into a low free energy state, and the new phase will have a certain radius defined by the super-saturation. Solubility of rare gas atoms in uranium alloys or ceramics is so low that it has not been measured. In perfect crystals, the order of magnitude of the solubility has been estimated to be 10^{-10} [10]. This figure may be increased up to $\approx 10^{-5}$ in the vicinity of dislocations. In addition, there may be a substantial effect from gas in dynamic solution, i.e., due to irradiation-induced re-solution. Thus, in regions of nuclear fuels that are near irradiation produced defects and/or various microstructural irregularities, the solubility of the gas can be substantially higher than in the bulk material. The gas concentration in these regions will increase until the solubility limit is reached, whereupon the gas will precipitate into bubbles. Subsequently, nucleation ceases due to the gas concentration in solution falling below the solubility limit. This is in stark contrast to the two-atom nucleation mechanism which is continuous from startup to the end of the irradiation. The trapping of the gas by the nucleated bubble distribution damps the increase in gas concentration. Eventually, the gas in solution may reach the solubility limit at which time the nucleation event repeats. Thus, assuming that all the gas precipitates into bubbles of equal size r', the concentration of gas in the bubble at nucleation is given by

$$m(r') = \frac{b_v c_g^{crit}}{4/3\pi r'^3 c_b(r')}, \tag{2}$$

where c_g^{crit} is the concentration of gas at the solubility limit, b_v is the volume per atom (Van der Waals constant), and $c_b(r')$ is the concentration of bubble nuclei at the unrelaxed radius r', i.e., the initial stage of bubble nucleation is a volume conserving process. Subsequently, in order to lower the free energy of the system, the overpressurized nuclei relax by absorbing vacancies until the bubbles reach equilibrium. At equilibrium, the bubble radius is r and, in the absence of significant external stress, the pressure in the bubble is given by

$$P_e(r) = \frac{2\gamma}{r}, \tag{3}$$

where γ is the surface energy per unit area. If it is assumed that the average gas-bubble size r' is a function of the equilibrium bubble size, then differentiating Eq. (2) with respect to the equilibrium radius r and rearranging terms yields,

$$\frac{1}{c_b(r')}\frac{dc_b(r')}{dr} = -\frac{1}{m(r')}\frac{dm(r')}{dr} - \frac{3}{r'}\frac{dr'}{dr}. \tag{4}$$

Let us assume that during the relaxation phase there is no interaction between the nucleated bubbles, i.e.,

$$r' \to r;\ m(r') \to m(r) = m(r'), \quad c_b(r') \to c_b(r) = c_b(r'). \tag{5}$$

The nucleation problem thus consists of determining the two terms on the right hand side (RHS) of Eq. (4). The first term on the RHS of Eq. (4) can be determined from the equation of state (EOS), the capillarity relation, and the conditions expressed in Eq. (5). Using the Van der Waals EOS,

$$P(V - mb_v) = mkT, \tag{6}$$

where $V = 4/3\pi r'^3$ is the bubble volume. Recognizing that at nucleation the bubble size is small such that $2\gamma/r' \gg \sigma$, where σ is the external stress and differentiating Eq. (6) with respect to the equilibrium radius r one obtains

$$\frac{1}{m(r')}\frac{dm(r')}{dr} = \frac{3}{r}\left[1 - \frac{rkT}{3(rkT + 2\gamma b_v)}\right]. \tag{7}$$

The remaining term on the RHS of Eq. (4) can be determined by invoking energy minimization as the driving force for bubble equilibration. The change in the Gibbs free energy due to bubble expansion is given by

$$\Delta G = \frac{4}{3}\pi r'^3 \Delta G_v + 4\pi r'^2 \gamma, \tag{8}$$

where ΔG_v is the free energy driving bubble equilibration, which, in analogy with the treatment of the nucleation of liquid droplets in a vapor [11], can be expressed as

$$\Delta G_v = \frac{kT}{\Omega}\ln(P_e(r)/P(r')), \tag{9}$$

where Ω is the atomic volume. The critical bubble radius at equilibrium is given by the condition

$$\frac{\partial \Delta G}{\partial r} = 0 \to r = r_{crit} = \frac{-2\gamma}{\Delta G_v}. \tag{10}$$

Inserting the expressions for P_e and P from Eqs. (3) and (6), respectively, into Eq. (10), differentiating with respect to the bubble radius r, and applying a little algebra results in

$$4\pi r'^2 \frac{dr'}{dr} = -\frac{1}{X}\left(\frac{\Omega}{r} + \frac{kT}{2\gamma}\right), \tag{11}$$

where

$$X = \frac{kTr}{2\gamma\left(\frac{4}{3}\pi r'^3 - mb_v\right)}. \tag{12}$$

Making use of Eq. (2) in Eq. (11) results in

$$\frac{3}{r'}\frac{dr'}{dr} = -\frac{m^2 c_b}{b_v c_g}\left[e^{2\gamma\Omega/rkT}\left(\frac{rkT}{2\gamma m}\frac{dm}{dr} + \frac{kT}{2\gamma} - \frac{\Omega}{r}\right) + \frac{b_v}{m}\frac{dm}{dr}\right]. \tag{13}$$

Finally, substituting Eqs. (5), (7), and (13) into Eq. (4) yields

$$\frac{1}{c_b}\frac{dc_b}{dr} = -\frac{1}{m}\frac{dm}{dr} + \frac{mc_b}{b_v c_g}\left[e^{2\gamma\Omega/rkT}\left(\frac{rkT}{2\gamma m}\frac{dm}{dr} + \frac{mkT}{2\gamma} - \frac{m\Omega}{r}\right) + b_v\frac{dm}{dr}\right]. \tag{14}$$

The as-nucleated bubble-size distribution is then obtained by the simultaneous solution to Eqs. (7) and (14).

Subsequent to the nucleation event, the as-nucleated bubble-size distribution evolves under the driving forces of gas diffusion to bubbles, gas-atom re-solution from bubbles, and bubble coalescence due to bubble–bubble interaction via bubble motion and geometrical contact. As stated above, additional nucleation events are delayed due to the gas in solution remaining below the solubility limit as the gas generated by continuing fission events is trapped within the existing bubble-size distribution. This last point is facilitated by the relatively high gas-atom diffusivities at the temperatures of interest (i.e., those under which the equilibrium γ-phase of the alloy exists). Eventually, the gas in solution may again reach the solubility limit at which time the nucleation event repeats.

3. Calculation of the fission-gas bubble-size distribution

The model consists of a set of coupled nonlinear differential equations for the intragranular concentration of fission-product atoms and gas bubbles of the form [12].

$$\frac{dC_i}{dt} = -a_i C_i C_i - b_i C_i + c_i (i = 1, \ldots, N), \tag{15}$$

where C_i is the number of bubbles in the i-th size class per unit volume; and the coefficients a_i, b_i and c_i obey functional relationships of the form

$$a_i = a_i(C_i), \quad b_i = b_i(C_1, \ldots, C_{i-1}, C_{i+1}, \ldots, C_N), \quad c_i = c_i(C_1, \ldots, C_{i-1}, C_{i+1}, \ldots, C_N). \tag{16}$$

The variables in Eq. (15) are defined in Table 1. a_i represents the rate at which bubbles are lost from (grow out of) the i-th size class because of coalescence with bubbles in that class; b_i represents the rate at which bubbles are lost from the i-th size class because of coalescence with bubbles in other size classes and re-solution; and c_i represents the rate at which bubbles are being added to the i-th size class because of fission gas generation, bubble nucleation, bubble growth resulting from bubble coalescence, and bubble shrinkage due to gas atom re-solution.

4. Bubble coalescence

The bubbles are assumed to diffuse randomly through the solid alloy by a volume diffusion mechanism. Bubble diffusion by a surface diffusion mechanism is also viable. However, the data available at the present time do not allow differentiation between the two mobility mechanisms. The bubble diffusion coefficient D_i of a bubble having radius R_i is given by

$$D_i = \frac{3a_0^3 D_{vol}}{4\pi R_i^3}, \tag{17}$$

Table 1
Definition of variables in Eq. (15), $\frac{dC_i}{dt} = -a_i C_i C_i - b_i C_i + c_i (i = 1, \ldots, N)$.

i	C_i	$a_i C_i C_i$	$b_i C_i$	c_i
1	Concentration of intragranular gas atoms	Rate of gas atom loss due to gas bubble nucleation	Rate of gas atom loss due to diffusion into gas bubbles	Rate of gas atom gain due to atom re-solution and fission of uranium nuclei
2, …, N	Concentrations of intragranular gas bubbles	Rate of gas bubble loss due to bubble coalescence with bubbles within the same size class	Rate of gas bubble loss due to coalescence with bubbles in other size classes	Rate of gas bubble gain due to bubble nucleation and coalescence, and diffusion of gas atoms into bubbles

where a_0 is the lattice constant and D_{vol} is the volume self-diffusion coefficient of the most mobile species in the alloy. The coefficients a_i and b_i (e.g. the 1st and 2nd terms on the RHS of Eq. (15)) are represented, respectively, by

$$a_i = 16\pi R_i D_i;\ b_i = \sum_{j\neq i}(R_i + R_j)(D_i + D_j)C_j. \tag{18}$$

The interaction cross-section represented in Eq. (18) is based on an analysis of colloidal suspensions within the framework of continuum theory [13]. Fission-gas bubbles can also interact due to mobility from biased motion within a temperature gradient. This aspect of the problem is handled in an analogous manner and will not be considered here.

As the bubbles grow and interact, the average spacing between bubbles shrink. In addition, as seen from Eq. (16), for the volume diffusion mechanism, bubble mobility falls off as the inverse of the radius cubed such that, for all practical purposes, relatively large bubbles are immobile. As the larger bubbles grow due to accumulation of the continual production of gas due to fission, the bubbles intercept other bubbles and coalesce. This process is here termed geometrical coalescence. For spherical bubbles that are all the same size and that are uniformly distributed, contact is reached when

$$2R_b(2C_b/3)^{1/3} = 1. \tag{19}$$

In analogy with percolation theory, the probability of an i-bubble contacting a j-bubble is given by

$$P_{ij}^{gc} = 0.5(1 - Erf[(1 - R_{ij}C_{ij}^{1/3})\sqrt{0.5}/\sigma]), \tag{20}$$

where

$$R_{ij} = R_i + R_j;\ C_{ij}^{1/3} = \left[\frac{2}{3}(C_i + C_j)\right]^{1/3}. \tag{21}$$

and σ is the width of the distribution that characterizes divergences from spherical bubbles and the uniform distribution assumption. In principle, σ is a measurable parameter.

The a_i and b_i coefficients in Eq. (18) now have an additional term given by

$$\begin{aligned} a_i^{gc} &= 4\pi D_{vol} R_i P_{ii} \\ b_i^{gc} &= 4\pi D_{vol} \sum_{j\neq i} R_i C_j P_{ij}, \end{aligned} \tag{22}$$

where P_{ij} is given by Eq. (20).

In what follows it is assumed that $D_{Xe} = D_{vol}$.

5. Analysis of U–10Mo high-temperature irradiation data

Fig. 2 shows the as-nucleated bubble-size distribution made with the simultaneous solution of Eqs. (7) and (14) for a gas-solubility of 10^{-7} at a fuel temperature of 850 K. At a fission rate of 1×10^{20} fissions $m^{-3}s^{-1}$, the solubility limit is reached in approximately 140 s. Subsequently, nucleation is limited due to the gas concentration in solution falling below the solubility limit. The trapping of gas in solution by the nucleated gas bubbles damps the rate at which the generated gas increases the gas concentration in dynamic solution. It is important to point out that here the solubility limit is an unknown parameter. If the solubility limit were 10^{-6} or 10^{-5}, the initial bubble nucleation event would occur after 1400 or 14,000 s of irradiation, respectively.

Fig. 3 shows m plotted as a function of r obtained from the solution of Eq. (7) for $T = 850$ K and $\gamma = 0.5$ Jm^{-2}. As expected from the form of Eq. (7), the number of gas atoms grows exponentially with bubble size. Fig. 4 shows the amount of gas in bubbles as a function of bubble size corresponding to Figs. 2 and 3. As is evident from Fig. 4, although the bubble-size distribution shown in Fig. 2 is relatively broad, the majority of the gas generated prior to the nucleation event (i.e., within the first 140 s of irradiation) exists in bubbles having radii less than 1 nm.

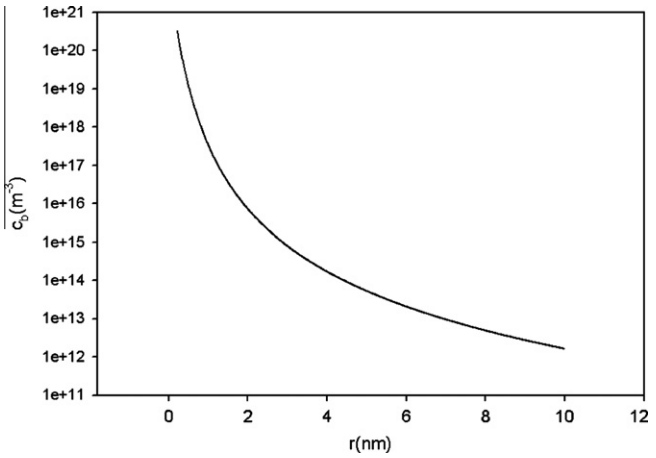

Fig. 2. As-nucleated bubble-size distribution made with the simultaneous solution of Eqs. (7) and (14) for a gas-solubility of 10^{-7}.

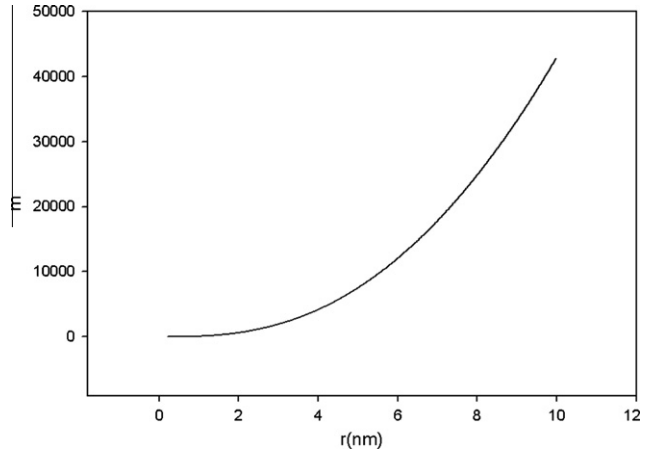

Fig. 3. Number of gas-atoms in a freshly nucleated bubble vs. bubble radius corresponding to Fig. 2.

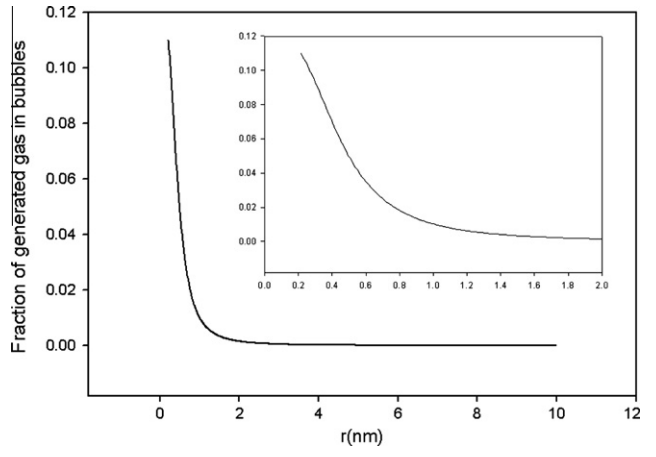

Fig. 4. Fraction of generated gas in bubbles vs. bubble radius corresponding to Figs. 2 and 3.

As discussed above, subsequent to the multi-atom bubble nucleation event, the concentration of gas in solution stays below the solubility limit due the trapping effect of the nucleated gas-bubbles such that additional multi-atom nucleation events are delayed. Thus, until the solubility limit is again exceeded, for the situation shown in Figs. 2–4, for irradiation times >140 s the bubble distribution follows from the evolution of the as-nucleated distribution shown in Fig. 2 due to bubble–bubble coalescence, and diffusion of generated gas to the existing bubble population. When the solubility limit is again exceeded, additional nucleation events occur within the evolving bubble population, and this complex of bubbles again evolves under the driving forces of bubble coalescence, gas-atom diffusion to, and gas-atom re-solution from bubbles.

Fig. 5 shows the calculated bubble-size distribution for an irradiation in U–8Mo at 850 K to 4% U atom burnup using Eq. (15) and the multi-atom nucleation model described in Section 2 for three values of the rare-gas solubility. The calculations shown in Fig. 5 were made using a gas-atom diffusivity, and re-solution rate given by

$$D_{vol} = 2 \times 10^{-4} e^{-33{,}000/kT}\ \mathrm{cm}^2\ \mathrm{s}^{-1}; \tag{23}$$

$$b = 1 \times 10^{-18} \dot{f}, \tag{24}$$

where $\dot{f}$ is the fission rate. The value for D_{vol} given in Eq. (23) is about a factor of 10 less than the out of pile measured U self-diffusion coefficient in U–10Mo [14]. On the other hand, it is not clear what diffusion mechanism dominates gas behavior in these alloys. For example, the Mo self-diffusion coefficient in U–10Mo is about an order of magnitude less than the U self-diffusion coefficient [15]. In addition, it is not at all clear how these diffusion couple measurements extrapolate to lower temperatures (lowest diffusion couple temperature was 1073 K), and to an irradiation environment. The value for b in Eq. (24) is ≈ an order of magnitude less than estimated for UO_2 [16]. This value is consistent with estimated irradiation enhanced creep rates in U–10Mo, which are ≈ an order of magnitude less than for UO_2 [17]. These effects can be traced to a higher thermal conductivity in the metal alloy as compared to the metal oxide.

The irradiation data shown in Fig. 5 was converted to a volume density from the measured areal density [18] using the Saltykov method [19]. The error bars associated with the solid circle data points are unknown, but they are most certainly substantial for the smaller bubble sizes where undercounting errors are typical. In addition, the fuel experienced an end of life constraint of ≈ 10 mp (the effect of hydrostatic constraint on bubble size is included in the calculations). Given these uncertainties, the bubble-size distribution is relatively flat for bubbles having radii from ≈ 5 to 12 μm. As shown in Fig. 4, a solubility of ≈ 2.5×10^{-8} provides a plausible interpretation of the data.

Fig. 6 shows the dependence of the calculated bubble-size distribution on the value of D_{vol} for a gas solubility of 2.5×10^{-8} compared with the measured quantities. As seen from Fig. 6, not surprisingly, the value of D_{vol} has a reasonably strong effect on the calculated distribution.

It is of interest to compare the multi-atom nucleation model with conventional two-atom nucleation as expressed by the first term on the right hand side of Eq. (1). Fig. 7 shows the calculated bubble-size distributions for an irradiation in U–8Mo at 850 K o 4% U atom burnup using Eq. (15) and the two-atom nucleation model for three values of the nucleation factor compared with irradiation data. Also shown are results for two different values of the volume diffusion coefficient for $f_n = 10^{-3}$. It is clear from Fig. 7 that the two-atom nucleation model does not satisfactorily interpret the measured bubble-size distribution over a 6 order of magnitude range in f_n and two order of magnitude range in D_{vol}. Thus, comparing Figs. 5 and 7, the multi-atom nucleation model provides a

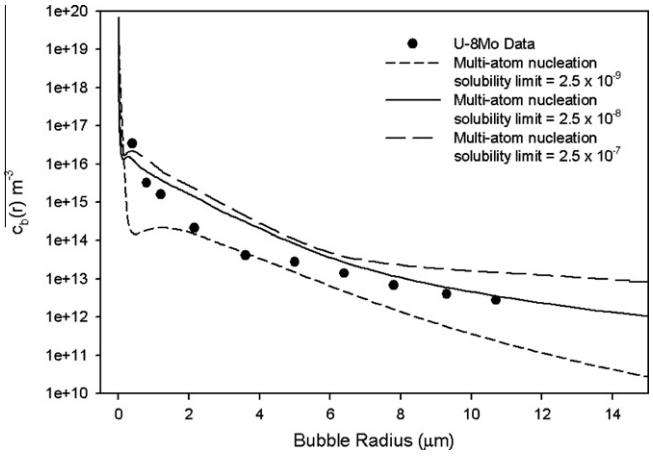

Fig. 5. Calculated bubble-size distributions for an irradiation in U–8Mo at 850 K to 4% U atom burnup using Eq. (15) and the multi-atom nucleation model described in Section 2 for three values of the rare-gas solubility compared with irradiation data.

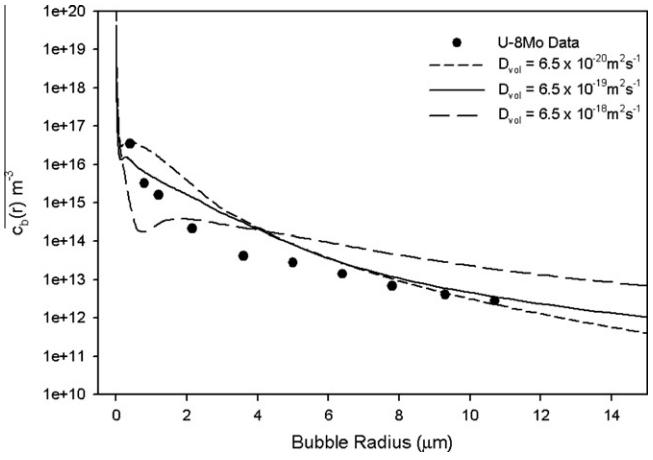

Fig. 6. Dependence of the calculated bubble-size distribution on the value of D_{vol} for a gas solubility of 2.5×10^{-8} compared with the measured quantities.

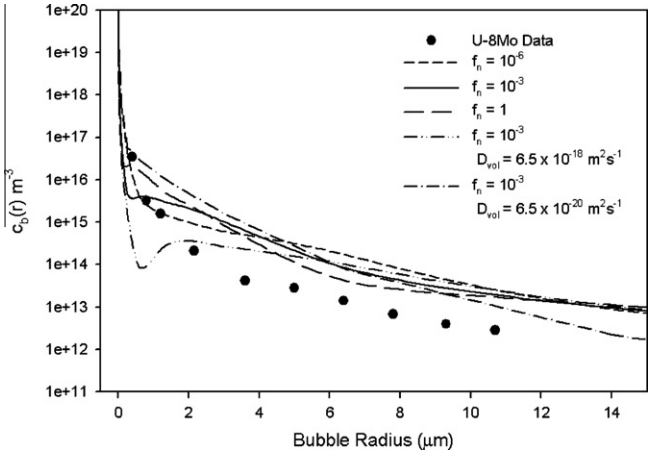

Fig. 7. Calculated bubble-size distributions for an irradiation in U–8Mo at 850 K to 4% U atom burnup using Eq. (15) and the two-atom nucleation model for three values of the nucleation factor compared with irradiation data. Also shown are results for two different values of the volume diffusion coefficient for $f_n = 10^{-3}$.

better interpretation of the data than the two-atom model. This becomes a stronger statement when the relatively insensitivity of the calculated tail of the distribution to the value of the nucleation factor and the volume diffusion coefficient for the two-atom model is compared to the "bracketing" of the data by commensurate changes in solubility and diffusion coefficient for the multi-atom model.

A more definitive differentiation between these two models requires data at a much lower burnup where the effects of bubble diffusion and coalescence are minimal. Unfortunately, such data are currently unavailable. Fig. 8 shows a comparison of multi-atom and two-atom nucleation mechanisms for an irradiation to 0.04% U burnup of U–8Mo fuel at 850 K. As shown in Fig. 8, the two-atom nucleation model leads to a substantially broader distribution than the multi-atom model. This feature is carried onto high burnup and, on comparing Figs. 5 and 7, is one of the key differences between these two nucleation models. It is anticipated that low burnup bubble distribution data will become available in the relatively near future [20]. Once this data becomes available, a more definitive differentiation between these two models can be undertaken.

6. Calculation of gas-driven fuel swelling safety margins

The model presented here, taken together with the analysis of fuel swelling in the low-temperature, irradiation-stabilized gamma phase [7] enable the calculation of gas-driven fuel swelling safety margins. Fig. 9 shows the calculated% unrestrained fuel swelling as a function of burnup for U–8Mo fuel irradiated at various temperatures. The calculated swelling is a strong function of the irradiation temperature as well as the fuel burnup. It should be noted that the temperature dependence of fuel that is under restraint (e.g. by cladding) is much softer than exhibited in Fig. 9.

The curves in Fig. 9 do not reflect any gas release that may occur. Empirically, gas release begins to occur when the swelling reaches 25–30% [21]. If all the bubbles are spherical, the same size, and randomly distributed then interconnection will be initiated at ≈ 33% swelling.

However, in general, the calculation of the swelling at which the bubbles interconnect is complicated by a relatively broad distribution of non-spherical bubbles, non-uniformly distributed within the fuel regions (e.g. such as that in Fig. 7). The maximum gas release in these high swelling fuels approaches 80%. There are many small bubbles in between the larger interconnected bubbles that continue to drive the swelling even at high gas release values (e.g. see Fig. 1). However, even so, the calculated swelling curves

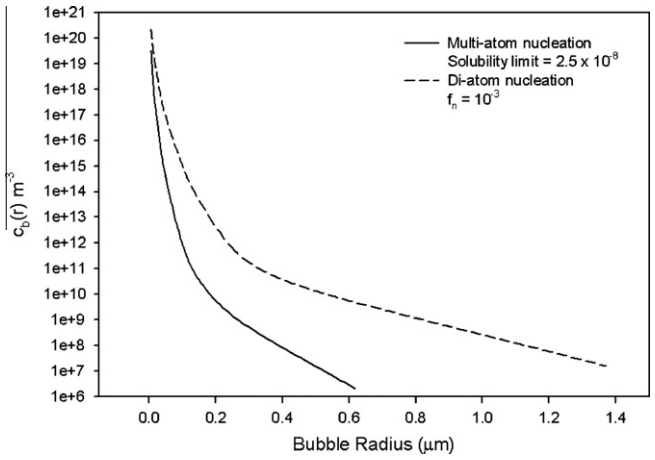

Fig. 8. Comparison of multi-atom and two-atom nucleation mechanism for irradiation to 0.04% U burnup in U–8Mo fuel at 850 K.

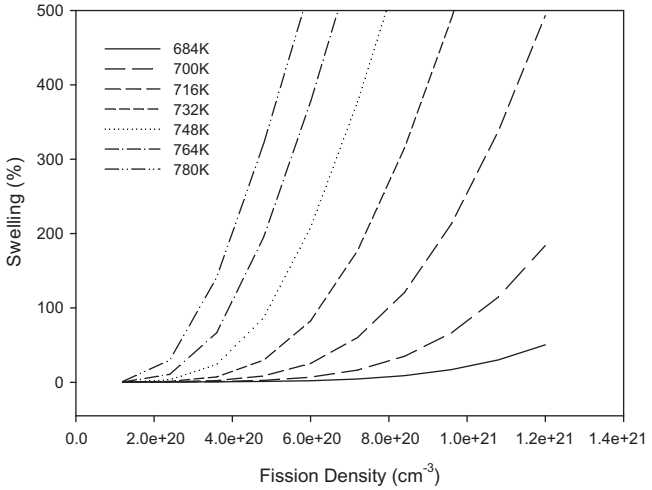

Fig. 9. Calculated unrestrained fuel swelling as a function of burnup and temperature.

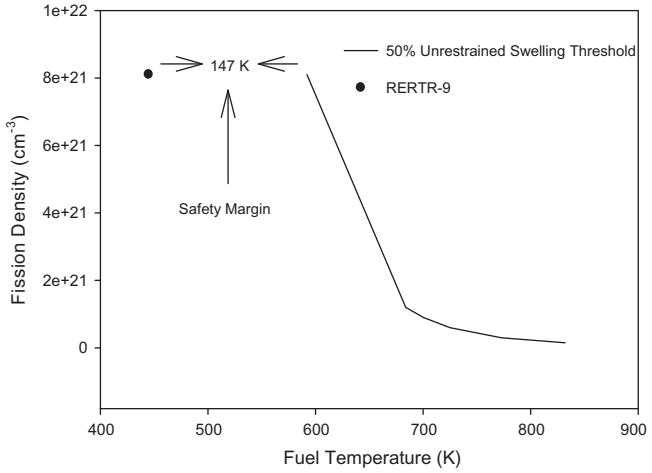

Fig. 10. Calculated threshold between stable and unstable gas-driven fuel swelling. Also shown is the fission density and fuel temperature for RERTR-9 [17].

in Fig. 9 are typical of those that have been measured [21]. The key here is that Fig. 9 is unrestrained swelling. If you give the fuel enough room it will keep on deforming.

If it is arbitrarily assumed that the maximum allowable fuel swelling is 50%, then fuel safety margins can be calculated using the results of Fig. 9. As an example of this type of calculation, Fig. 10 shows the calculated boundary between stable and unstable unrestrained fuel swelling as a function of fission density and fuel temperature. The solid line in Fig. 10 is the 50% unrestrained swelling threshold obtained from Fig. 9. Also shown in Fig. 10 is the fission density and fuel temperature for RERTR-9 [17]. As shown in Fig. 10, the calculated safety margin for RERTR-9 is ~150 K.

7. Conclusions

Analysis of different nucleation mechanisms in light of measured bubble-size distributions in U–8Mo fuel irradiated in the equilibrium gamma phase indicates that a multi-atom nucleation mechanism is operative. The conventional two-atom nucleation model is not consistent with the trends of the data. A more definitive test of the nucleation mechanism requires measured bubble distributions at a very low burnup.

The results demonstrate the increased validation leverage secured with the use of bubble-size distributions compared with the use of mean values (i.e., average quantities such as bubble density and diameter). Model predictions are sensitive to various materials and model parameters. Improved prediction capability requires an accurate quantification of these critical materials properties and measurement data. These uncertainties can be reduced when the availability of additional well-characterized bubble-size distributions obtained from fuel irradiated at several different temperatures becomes available. In addition, there are efforts underway to estimate values for certain critical parameters and materials properties using lower length scale, first-principle calculational methods [22].

The results of this analysis enable the calculation of safety margins for unrestrained fuel swelling. These safety margins contain an uncertainty primarily tied to uncertainties in the values of the volume and Xe diffusion coefficients.

Acknowledgements

The author would like to thank G.L. Hofman and Y.S. Kim for interesting discussions. The author would also like to thank. H.J. Ryu for his help in converting the data to volume density from the measured areal density using the Saltykov method.

References

[1] G. Hofman, J. Snelgrove, in: B.R.T. Frost (Ed.), Metallic Fast Reactor Fuels Materials Science and Technology, vol. 10, VCH, 1994.
[2] G.W. Greenwood, A.J.E. Foreman, D.E. Rimmer, J. Nucl. Mater. 4 (1959) 305.
[3] J.A. Turnbul, J. Nucl. Mater. 38 (1971) 203.
[4] A.D. Whapham, On the Formation of Gas Bubbles in Fissile Material During Reactor Irradiation, AERE-R 6595, 1970.
[5] M.H. Wood, K.L. Kear, J. Nucl. Mater. 118 (1983) 320.
[6] D.R. Olander, D. Wongsawaeng, J. Nucl. Mater. 354 (2006) 94.
[7] J. Rest, G.L. Hofman, Y.S. Kim, J. Nucl. Mater. 385 (2009) 563.
[8] A.E. Volkov, A.I. Ryazanov, J. Nucl. Mater. 273 (1999) 155.
[9] R.A. Jackson, C.R.A. Catlow, J. Nucl. Mater. 127 (1985) 161.
[10] J. Blin, CEA Report 1444, 1960.
[11] D. Turnbull, Solid State Phys. III (1956) 225–306.
[12] J. Rest, Grass-SST: A Comprehensive, Mechanistic Model for the Prediction of Fission-gas Behavior in UO_2-base Fuels during Steady-state and Transient Conditions, NUREG/CR-0202, ANL-78-53, 1978.
[13] E.E. Gruber, J. Appl. Phys. 38 (1967) 243.
[14] G.B. Fedorov, E.A. Smirnov, Diffusion in Reactor Materials, Oxonian Press Pvt. Ltd., New Delhi, 1984.
[15] Y. Adda, J. Philibert, Diffusion of uranium with some transition metals, in: Proc. 2nd United States Inter. Conf. on the Peaceful Uses of Atomic Energy, Geneva, Switzerland, 1958.
[16] J. Rest, J. Nucl. Mater. 321 (2003) 305.
[17] G.L. Hofman, Y.S. Kim, A.B. Robinson, Fission induced swelling and creep of uranium–molybdenum alloy fuel, in: Trans. 13th International Topical Meeting on Research Reactor Fuel Management, Vienna, 2009, ISBN: 978-92-95064-07-2.
[18] Bernard Kryger, Contribution A L'etude Du Degagement Des Gaz De Fission Dans Les Combustibles Nucleaires Metalliques, CEA-R-3888, 1969.
[19] R.T. DeHoff, F.N. Rhines, Quantitative Microscopy, McGraw-Hill, New York, 1968. pp. 162.
[20] G.L. Hofman, Private Communication, Argonne National Laboratory, October, 2009.
[21] Argonne National Laboratory/AEC Research and Development Report, ANL-7299, Metals, Ceramics and Materials, TID-4500, 1966.
[22] Z. Insepov, J. Rest, G.L. Hofman, A. Yacout, G.E. Norman, S.A. Starikov, V.V. Stegailov, A new multiscale approach to nuclear fuel simulations: atomistic validation of kinetic method, presented at the Embedded Topical Meeting on Nuclear Fuels and Structural Materials for the Next Generation Nuclear Reactors, 2010 ANS Annual Meeting, San Diego, CA, June 13–17, 2010.